Fixed boundary toroidal plasma equilibria with toroidal flows

Yanqiang Hu, Yemin Hu, and Nong Xiang

Citation: Physics of Plasmas **23**, 042506 (2016); doi: 10.1063/1.4947028
View online: http://dx.doi.org/10.1063/1.4947028
View Table of Contents: http://aip.scitation.org/toc/php/23/4
Published by the American Institute of Physics

Fixed boundary toroidal plasma equilibria with toroidal flows

Yanqiang Hu,[1,2,3] Yemin Hu,[1,3] and Nong Xiang[1,3]
[1]*Institute of Plasma Physics, Chinese Academy of Sciences, Hefei 230031, China*
[2]*University of Science and Technology of China, Hefei 230026, China*
[3]*Center for Magnetic Fusion Theory, Chinese Academy of Sciences, Hefei 230031, China*

(Received 5 January 2016; accepted 31 March 2016; published online 18 April 2016)

The fixed boundary toroidal plasma equilibria with toroidal flows are investigated by solving the modified Grad-Shafranov equation numerically in the cylindrical coordinate system. For normal equilibrium configurations with geometry and profiles similar to usual tokamaks with no flow, it is found that the effect of flow is to lead to an outward shift of the magnetic flux surfaces, together with the profiles of pressure, and mass and current densities. The shifts could become significant when the toroidal flow Mach number exceeds 0.5. For non-conventional current profiles, even for the usual tokamak geometry, novel current reversal equilibrium configurations may result, sometimes with changed topology in the poloidal flux function. This change in the topology of plasma equilibrium can be attributed to the large toroidal flow. The computed results may correspond to situations of intense tangential injection during the low toroidal current phase in expected experimental situations. *Published by AIP Publishing.* [http://dx.doi.org/10.1063/1.4947028]

I. INTRODUCTION

Plasma flows (rotations) have been observed in many tokamaks,[1–7] particularly in neutral beam heating experiments.[2–4,8] Studies of the equilibrium and stability properties of rotating plasmas have recently attracted considerable interest in fusion plasma research.[1,7] The plasma rotation could be spontaneous or driven by neutral beam injection or radio-frequency wave heating. In certain phases of the discharge, both the energy transport and the macroscopic stability are significantly impacted by either the poloidal or toroidal plasma rotations.

We note that there are already a rich history on the investigations of the effect of plasma flow and flow shear on the plasma equilibrium[1,9–14] in the literature. The general equilibrium result is that a large plasma flow, with a significant Mach number (defined as the velocity of flow relative to the sound speed or the Alfven velocity) will lead to a significant outward shift of the magnetic surfaces, accompanied by the shifts in the profiles of the pressure and mass and current densities. Together with these are the investigations on the effect of flow on the macroscopic plasma stabilities such as the internal and external kinks,[15–17,20] ballooning modes,[18,19] and resistive wall Mode (RWM)[20–22] etc. In recent years, it has been observed in several tokamaks that the existence of sheared toroidal flows in the equilibrium could have a beneficial influence on the neoclassical tearing modes (NTMs).[23] Impurity transport is also strongly correlated with toroidal plasma rotation. The injection of fast, neutral particles which parallel to the plasma current (coinjection) suppresses the accumulation of impurities in the center of the plasma, and while in the case of counterinjection, the impurity buildup is enhanced.[24] However, very large rotation is also found to be unfavorable for plasma stability. It is found that the kink mode may be destabilized by high rotation velocities, even when the safety factor at the magnetic axis is above unity.[25] On the other hand, as far as the poloidal flow is concerned, a large poloidal flow could cause the governing equation determining the plasma equilibrium configurations to become hyperbolic, introducing internal discontinuities into the pressure profiles in the plasma. This would require the existence of shock waves on the plasma sources which might lead to equilibrium degradation.[26] On the one hand, the study of stability and transport requires first accurate knowledge about the plasma equilibrium. On the other hand, we still find challenging and interesting issues on the accurate determination of the complete knowledge on plasma equilibrium. This work is thus motivated by having a better understanding of the issue of toroidal plasma equilibrium with a toroidal flow.

The generalized Grad-Shafranov (GGS) equation of a rotating plasma was first given concisely by Hameiri.[10] Maschke and Perrin showed that with some simplifying assumptions,[9] the GGS equations can be solved analytically. Recently, Guazzotto *et al*. have investigated numerically the effects of toroidal and poloidal flows on the equilibrium of tokamak plasmas by using the equilibrium code FLOW.[1] Their results covered a wide range of tokamak equilibria, but apparently with the plasma configuration mainly consisted of nested flux surfaces.

In this work, we concentrate our attention on plasma with a pure toroidal flow. We first formulate and define the equilibrium problem under consideration. The GGS equation with toroidal flow is solved in a fixed domain without first assuming the equilibrium to consist of nested flux surfaces. The solution method is to first divide the domain into triangular sub-regions, and the solution in each sub-region is assumed to be spanned by a finite element. The sub-regions can be refined to consist of finer sub-regions. The nonlinear GGS equation is then cast into a matrix equation for the poloidal flux function with given sources. The matrix equation is solved iteratively with the source functions determined by the previous iteration. The convergence is tested self-consistently by demanding that the solution converge to

a specific accuracy. We first calibrate our numerical results against the analytic solution. We then investigated the effect of a toroidal flow on a normal equilibrium configuration (NEC), choosing for the plasma boundary similar to that of Experimental Advanced Superconducting Tokamak (EAST). We fixed the toroidal current in the equilibrium solution and showed that as previous authors found, the effect of toroidal flow is mainly to impart an outward shift to the plasma flux surfaces, together with the pressure, and mass and current density profiles. The shifts are especially prominent when the Mach number is larger than 0.5. It also has effects on the total β_v, normalized β_N, and volume average pressure p_v.

We next study the current reversal equilibrium configurations (CRECs), and these are equilibria with unconventional plasma current profiles. CRECs have been demonstrated to exist experimentally as well as theoretically[27–34] in plasmas without flow or with small flow. Experiments on JET and JT-60 have demonstrated improved confinement regimes with reversed shear and nearly zero toroidal current density in the central region. On the other hand, alternating-current operation has been demonstrated experimentally on several tokamaks such as Stor-1M, CT-6B, and HT-7. By fixing other constants in the plasma equilibrium profile and increasing only the Mach number, we showed that for very low current equilibria, the configuration can change from NEC to CREC. Thus toroidal plasma flow is the direct cause of these CRECs. This could correspond to intense tangential neutral beam injection during the initial low current phase of the tokamak discharge. We next show that change in discharge topology due to plasma rotation can be further demonstrated starting with a CREC and changed into another type of CREC.

The paper is organized as follows: In Sec. II, the formulation of the problem of plasma equilibrium with a toroidal flow in a fixed domain is presented. We also give a brief discussion of the method of solution. Details of the results of numerical solution are given in Sec. III. We first discuss the validation of our results and the results of solutions for the NECs in Sec. III A. The discussion on the possibility of changes in plasma topology is presented in Sec. III B. A brief discussion and summary is given in Sec. IV.

II. FORMULATION OF THE FIXED BOUNDARY EQUILIBRIA FOR PLASMA WITH TOROIDAL FLOW AND METHOD OF SOLUTION

We start with the ideal magnetohydrodynamics (MHD) equations for a toroidally rotating plasma and use the standard cylindrical coordinates (r, φ, z). Where r is the major radius of the torus, φ the toroidal angle, and z the height above the midplane. For the toroidally symmetric plasma equilibrium, $\frac{\partial}{\partial \varphi} = 0$. The basic MHD equations include the equations for (1) mass and (2) momentum conservation, as well as the Maxwell's equations (3)–(5) written in the following standard form:[10]

$$\nabla \cdot (\rho \boldsymbol{v}) = 0, \tag{1}$$

$$\rho \boldsymbol{v} \cdot \nabla \boldsymbol{v} = -\nabla p + \boldsymbol{J} \times \boldsymbol{B}, \tag{2}$$

$$\nabla \cdot \boldsymbol{B} = 0, \tag{3}$$

$$\mu_0 \boldsymbol{J} = \nabla \times \boldsymbol{B}, \tag{4}$$

$$\nabla \times (\boldsymbol{v} \times \boldsymbol{B}) = 0, \tag{5}$$

$$\boldsymbol{v} \cdot \nabla S = 0, \tag{6}$$

$$p = S\rho^{\gamma}, \tag{7}$$

where ρ, v, p, J, B, and γ are the plasma density, velocity, pressure, current density, magnetic field, and the adiabatic constant. Eq. (6) is the equation for the specific entropy S, and Eq. (7) is the equation of state for plasma pressure p.

It is well known that the magnetic field can be written as

$$\boldsymbol{B} = \nabla\psi \times \nabla\varphi + \boldsymbol{B}_{\varphi}\boldsymbol{e}_{\varphi}, \tag{8}$$

where $\psi(r, z)$ is the poloidal flux function. From Eq. (5), we obtain

$$\boldsymbol{v} \times \boldsymbol{B} = \nabla\Theta. \tag{9}$$

Because $\nabla\Theta$ is perpendicular to B, $\nabla\Theta = \Omega(\psi)\nabla\psi$, where $\Omega(\psi)$ is an arbitrary function of the poloidal flux ψ. Ignoring the poloidal flow, we obtain

$$v = v_{\varphi} = r\Omega. \tag{10}$$

Therefore, Ω is the toroidal rotation angular frequency of the flux surface. From Eqs. (6) and (10), we could find that S can be an arbitrary axially symmetric function of r and z. For simplicity, we assume

$$S = S(\psi). \tag{11}$$

Note this choice is not arbitrary. Rather, it corresponds to the general behavior of the entropy function S in a plasma with a general flow, including the aligned flow. In our present case, the aligned flow has been damped to a negligible value. From the φ component of the momentum equation (2), we get $\boldsymbol{B} \cdot \nabla(rB_{\varphi}) = 0$, which implies

$$B_{\varphi} = \frac{\mu_0 F(\psi)}{r}, \tag{12}$$

here $F(\psi)$ is an arbitrary function of the poloidal flux. We note this relation is the same as the case of plasma equilibrium without flow. From the well known thermodynamic relations

$$dw = \frac{1}{\rho}dp + TdS, \tag{13}$$

where ω and T are the specific enthalpy and plasma temperature. Because the differential operator d in (13) stands for change in the plasma frame, we can use Equations (6) and (11) to obtain

$$\frac{1}{\rho}\nabla p = \nabla w, w = \frac{\gamma}{\gamma - 1}S\rho^{\gamma - 1}. \tag{14}$$

Multiplying the moment equation (2) by $\frac{1}{\rho}\vec{B}$ and using (14), we can get another equation of the form $\vec{B} \cdot \nabla f = 0$, yielding

$$-\frac{r^2}{2}\Omega^2+\frac{\gamma}{\gamma-1}S\rho^{\gamma-1}=H(\psi), \tag{15}$$

where $H(\psi)$ is a arbitrary function. This is the analog of Bernoulli's law in fluid dynamics. In the same way, the $\nabla\psi$ component of the momentum equation yields[9–12]

$$-\nabla\cdot\left(\frac{1}{r^2}\nabla\psi\right)=\mu_0\left[(\rho r v_\varphi)\frac{d\Omega}{d\psi}+\frac{B_\varphi}{r}\frac{dF}{d\psi}+\rho\frac{dH}{d\psi}-\frac{\rho^\gamma}{\gamma-1}\frac{dS}{d\psi}\right]=\frac{j_\varphi}{r}. \tag{16}$$

In summary, collecting Eqs. (12), (15), and (16), we have obtained the following set of equations:

$$B_\varphi=\frac{\mu_0 F(\psi)}{r}, \tag{17}$$

$$-\frac{r^2}{2}\Omega^2+\frac{\gamma}{\gamma-1}S\rho^{\gamma-1}=H(\psi), \tag{18}$$

$$-\nabla\cdot\left(\frac{1}{r^2}\nabla\psi\right)=\mu_0\left[(\rho r v_\varphi)\frac{d\Omega}{d\psi}+\frac{B_\varphi}{r}\frac{dF}{d\psi}+\rho\frac{dH}{d\psi}-\frac{\rho^\gamma}{\gamma-1}\frac{dS}{d\psi}\right]. \tag{19}$$

These constitute the generalized Grad-Shafranov (GGS) equations of a plasma with toroidal rotation. Here, we assumed that the entropy is constant on the magnetic surface. The solution depends on the four arbitrary functions of $\psi:\Omega,F,H,S$. It is a nonlinear elliptic partial differential equation defined over a closed domain.

We further adopt the following dimensionless parameters to cast the GGS equations into a nondimensional form.

$$x=\frac{r}{a},\quad z=\frac{z}{a},\quad S\to\frac{S}{S_0},\quad H\to\frac{H}{H_0},$$
$$\Omega\to\frac{\Omega}{\Omega_0},\quad F\to\frac{F}{F_0},\quad \rho\to\frac{\rho}{\rho_0},\quad p\to\frac{p}{p_0},$$
$$\psi\to\frac{\psi}{\psi_0},\quad B_\varphi\to\frac{B_\varphi}{B_0},\quad v_\varphi\to\frac{v_\varphi}{v_0},$$
$$\psi_0=B_0a^2,\quad j_\varphi\to\frac{j_\varphi}{j_0},\quad j_0=\frac{B_0}{a},$$
$$F_0=\frac{aB_0}{\mu_0},\quad S_0=\frac{B_0^2}{\mu_0\rho_0^\gamma},\quad H_0=\frac{B_0^2}{\mu_0\rho_0}=v_{A0}^2,$$
$$p_0=S_0\rho_0^\gamma=\frac{B_0^2}{\mu_0},\quad v_0=R_0\Omega_0,$$

where B_0,ρ_0,Ω_0 are the value of magnetic field, plasma density, and toroidal rotation frequency at $r=R_0$, which is chosen to be at the center of the computational domain. R_0,a are the major radius and the minor radius.

Using the above dimensionless parameters, we rewrite Eqs. (17), (18), and (19) as

$$B_\varphi=\frac{F}{x}, \tag{20}$$

$$-\frac{1}{2}\varepsilon^2M_{t0}^2x^2\Omega^2+\frac{\gamma}{\gamma-1}S\rho^{\gamma-1}=H, \tag{21}$$

$$\nabla\cdot\left[\frac{1}{x^2}\nabla\psi\right]+\varepsilon M_{t0}^2x\rho v_\varphi\frac{d\Omega}{d\psi}+\frac{B_\varphi}{x}\frac{dF}{d\psi}+\rho\frac{dH}{d\psi}-\frac{\rho^\gamma}{\gamma-1}\frac{dS}{d\psi}=0. \tag{22}$$

Here, $\varepsilon=\frac{1}{x_0},x_0=\frac{R_0}{a}$. $M_{t0}=\frac{v_0}{v_{A0}}$ is the reference Alfven Mach number. From Eq. (21), the density can be solved analytically. Then, we obtain

$$\rho=D\left[1+\frac{\gamma-1}{2}\varepsilon^2M_{t0}^2(\varepsilon^2x^2-1)M^2\right]^{\frac{1}{\gamma-1}},$$
$$M=\frac{x_0\Omega}{C_s},\quad C_s=\sqrt{\frac{\gamma P}{D}}, \tag{23}$$

where

$$D=\left[\frac{\gamma-1}{S\gamma}\left(H+\frac{1}{2}M_{t0}^2\Omega^2\right)\right]^{\frac{1}{\gamma-1}}, \tag{24}$$

which can be viewed as a "quasi-density". The free functions Ω,F,H,S are then the same as those in Ref. 1

$$F(\psi)=x_0B_t(\psi), \tag{25}$$

$$\Omega(\psi)=\sqrt{\frac{\gamma P}{D}}\frac{M}{x_0}, \tag{26}$$

$$H(\psi)=\frac{\gamma P(\psi)}{D(\psi)}\left(\frac{1}{\gamma-1}-\frac{1}{2}\varepsilon^2M_{t0}^2M_\varphi^2\right), \tag{27}$$

$$S(\psi)=\frac{P(\psi)}{D(\psi)^\gamma}, \tag{28}$$

where B_t,M,P,D can be viewed as "quasi-toroidal magnetic field," "quasi-toroidal Mach number," "quasi-pressure," and "quasi-density," respectively. Defining these free functions facilitates the assignment of the input parameters for the numerical solution of the GGS equation(s).

To continue the specification of the fixed boundary equilibrium problem, we adopt the Dirichlet boundary condition of $\psi=0$ on the boundary. Once the profile parameters are supplied, the GGS equation is solved iteratively over the computational domain. We note that usually, the GGS equation could be close to linear, then an integral constraint, such as the total plasma current needs to be supplied to ensure we do not obtain a null solution. On the other hand, after enough equilibrium profile data is supplied, the solution is determined self-consistently. Some of the global quantities, such as total poloidal flux, toroidal flux, and even the number of closed flux regions in the computational domain are then self-consistently determined by the solution. Because the profiles are inherently nonlinear, uniqueness of the solution is not guaranteed. Herein lies the possibilities of multiple solutions which could possibly be obtained by specifying the same profile parameters differently or adopt a different process for the solution of the problem.

We use the finite element method to solve the coupled equation set Eqs. (20), (21), and (22). The computation domain is covered by a triangular mesh with the basic region a

small triangle. The finite element base functions are defined on each of the triangular regions. The GGS equation is then recast into a matrix equation for the base (poloidal flux) functions on triangles. The highest order derivative term in the partial differential GGS equation is iteratively solved using the results from the previous equation to specify the source current terms. Iteration continues until the solution converges to a predetermined accuracy. After a converged solution is obtained, analysis is performed on it to obtain the desired information on the equilibrium.

After an initial checking against the analytic solutions given by Maschke and Perrin, we concentrate our numerical study on the normal equilibrium configurations (NECs), and then the current reversal equilibrium configurations for the Experimental Advanced Superconducting Tokamak (EAST)-like plasmas.

III. NUMERICAL RESULTS

In this section, we solve Eqs. (20), (21), and (22) by taking the EAST-like parameters as follows: (except in checking the analytic solution, we adopt a boundary consistent with that specified by the analytic solution)

$$R_0 = 1.85\,\mathrm{m}, \quad a = 0.45\,\mathrm{m}, \quad elong = 1.8, \quad \delta = 0.6,$$
$$B_0 = 2\,\mathrm{T}, \quad \gamma = 5/3, \quad P_e = 0, \quad P_0 = 0.02,$$
$$\mu_p = 2, \quad D_e = 0, \quad D_0 = 1,$$
$$\mu_D = 0.2, \quad B_{te} = 1, \quad \mu_B = 1,$$
$$M_e = 0, \quad \mu_M = 0.2, \quad M_{t0} = 1.$$

In the following figures, all the abscissas are the dimensionless quantity x, and if no special claim, the ordinate are the dimensionless quantity z.

We consider two kinds of equilibria: the normal equilibrium configurations (NECs) and the current reversal equilibrium configurations (CRECs).

A. Normal equilibrium configurations

For the normal flow equilibrium, we set B_t, M, P, D as the following analytic expression as in Ref. 1

$$B_t = B_{te} + (B_{t0} - B_{te})\left(\frac{\psi}{\psi_0}\right)^{\mu_B}, \tag{29}$$

$$M = M_e + (M_0 - M_e)\left(\frac{\psi}{\psi_0}\right)^{\mu_M}, \tag{30}$$

$$D = D_e + (D_0 - D_e)\left(\frac{\psi}{\psi_0}\right)^{\mu_D}, \tag{31}$$

$$P = P_e + (P_0 - P_e)\left(\frac{\psi}{\psi_0}\right)^{\mu_P}. \tag{32}$$

The subscripts e and 0 denote the values at the plasma boundary and $x = x_0$, respectively.

The roots of the Bernoulli equation (21) yield the plasma density ρ which should meet the condition $\rho \geq 0$, so from Eq. (23), we get the sufficient condition for the real root of ρ.

$$M \leq M_c = \frac{\sqrt{2}}{\varepsilon M_{t0}\sqrt{(\gamma-1)\varepsilon(2-\varepsilon)}}.$$

Using the above parameters for EAST, we obtain $M_c = 10.1$, and the corresponding actual Mach number $M_r = 2.46$.

1. Validation against analytic solution

First of all, in order to verify the validity of our numerical method, we made a benchmark comparison between the results from our numerical method and that from the analytical method. An exact solution of Eq. (22) was obtained by making the following assumptions:[9]

$$\frac{\Omega^2}{H} = \frac{w^2}{r_0^2}, \tag{33}$$

$$p_s = \frac{P_0}{r_0^4}(\psi - \psi_1), \tag{34}$$

$$F^2 = F_0^2 + 2\frac{\mathcal{F}}{r_0^2}(\psi - \psi_1), \tag{35}$$

where $w^2 = \frac{2M_0^2}{\frac{2}{\gamma-1}-M_0^2}$, $p_s(\psi) = (\frac{H}{\eta})^\eta S^{1-\eta}, \eta = \frac{\gamma}{\gamma-1}$, r_0 is a suitably chosen scale length, P_0, ψ_1, F_0 and $\mathcal{F}$ are the constants, and M_0 is the Mach number at $r = r_0$.

In the case of $\mathcal{F} = 0$, ψ_1 and F_0 need not to be specified. Eq. (22) becomes a linear partial differential equation for the function ψ and has the exact solution as the following form:[9]

$$\psi - \psi_0 = P_0\left\{\frac{Cr^2}{r_0^2} + \frac{\varepsilon_a - 1}{4}\frac{r^2}{r_0^2}\left(\frac{z^2}{r_0^2} - \frac{r^2}{4r_0^2}\right) + \frac{1}{(\eta+1)(\eta+2)w^4}\left[1 + (\eta+2)\frac{w^2r^2}{2r_0^2} - G^{\eta+2}\left(\frac{r}{r_0}\right)\right]\right\}, \tag{36}$$

where $G(\frac{r}{r_0}) = 1 + \frac{w^2r^2}{2r_0^2}$, $C = (\varepsilon_a - 1)\frac{r_a^2}{8r_0^2} - \frac{1-G^{\eta+1}}{2(1+\eta)\Omega^2}$, ε_a is a constant, and r_a is the magnetic axis.

Shown in Fig. 1 is the overlay of results from the two methods. Here, the solid and dash lines are the analytical and numerical solutions, respectively. In this figure, the outermost flux contours was taken as the outer-boundary of the computational domain with the flux function value of $\psi = 0$. The other two inner contours are for $\psi = 0.02$ and $\psi = 0.07$. Aside from the above mentioned parameters of $\varepsilon_a = 0$, $\eta = 5/2$, we have also taken $r_0 = r_a$, $M_0 = 1$ and $\psi_0 = -0.01$. It is readily seen that out numerical results of are in good agreement with the exact analytical calculations.

2. NECs in EAST-like configuration

To obtain the value of B_{t0}, we resort to the relationship of normalized total toroidal current $I = \int j_\varphi dxdz$, which is used as a constraint during the solution of the equilibrium equation. Here, we take $I = 1$, adjust the value of M_0, and then obtain the value of B_{t0} and M_{r0} (the value of the actual Mach number at $x = x_0$). The values are shown in Table I.

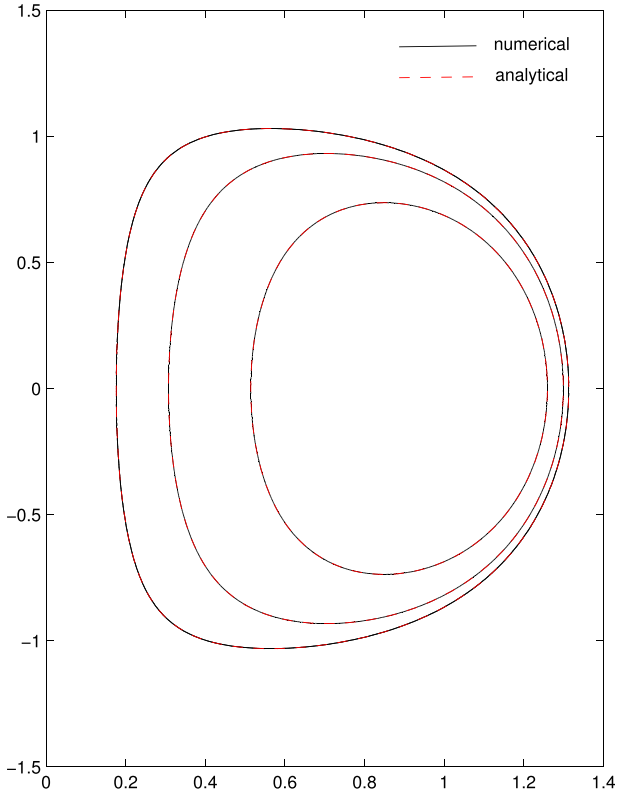

FIG. 1. Comparison of the flux function obtained from our numerical computation with that of the analytic solution given by Eq. (36).

In Fig. 2, the actual Mach number is defined as $M_r = \frac{v_\varphi}{c_s}, v_\varphi = r\Omega, c_s = \sqrt{\frac{\gamma p}{\rho}}$, where c_s is the sound speed. The actual Mach number can be obtained from the relationship

$$M_r = M_{t0}\frac{\varepsilon^2 x}{\sqrt{\mathcal{D}}}M, \tag{37}$$

where $\mathcal{D} = 1 + \frac{(\gamma-1)\varepsilon^2 M_{t0}^2}{2}(\varepsilon^2 x^2 - 1)M^2$.

As shown in Fig. 2, the Mach number profile is elevated by increasing the value of parameter M_{r0} from 0 to 0.7. And, Fig. 3 shows an increasing outward shift of the poloidal flux function and the magnetic axis with the increase in the Mach number profile. The shifts could be not obvious when the Mach number is much less than 0.5, while the shifts become quite prominent when the Mach number becomes larger than 0.5. In the experiments, the (real) Mach numbers of tokamaks has been observed to be about 0.1–0.5.[2–5] The achieved Mach number in the EAST is about 0.2. Therefore, the observed shifts of the magnetic axis due to the effects of rotation have not been prominent.

Figs. 4–7 show the change of the normalized density, pressure, β, toroidal current density across the midplane for varying toroidal flows in an EAST-like plasma. It is seen

TABLE I. M_{r0} and B_{t0} for different M_0.

M_{r0}	0	0.2	0.5	0.7
M_0	0	0.823	2.058	2.881
B_{t0}	1.0035	1.0029	0.9986	0.9929

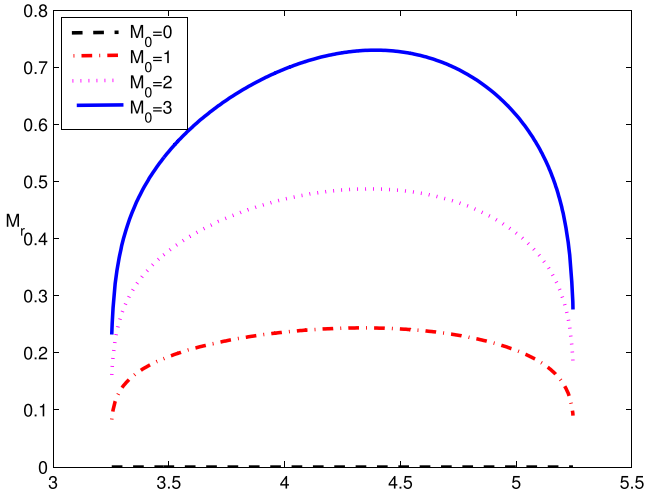

FIG. 2. Profiles of the actual toroidal Mach number M_{r0} across the midplane for different M_0.

that the most prominent consequence of the increasing rotation Mach number is the increasing outward shifts of the profiles of the density, the pressure, the local β, and the toroidal current density of the plasma column. Comparing the different profiles on their trend of change with respect to the change in the rotation Mach numbers, it is also found that the rate of change of the profiles with the change in Mach number started slow. The rate of change increases with the increase in rotation Mach numbers. Finally at large Mach numbers, we find the plasma is squeezed against the outboard side of the boundary by the centrifugal force. Since the boundary itself is fixed, this will result in higher peaks and steeper gradients of the profiles in the outboard region of the plasma. This holds true for the mass density, the pressure, the local β as well as the current density. These sharp gradients have been known to be the source of MHD instabilities.

In Fig. 7 and Table II, the $\beta, \beta_v, \beta_N, p_v$, and I_p are defined as follows:

$$\beta = \frac{2p}{B^2}, \quad \beta_v = \langle\beta\rangle, \quad p_v = \langle p\rangle,$$

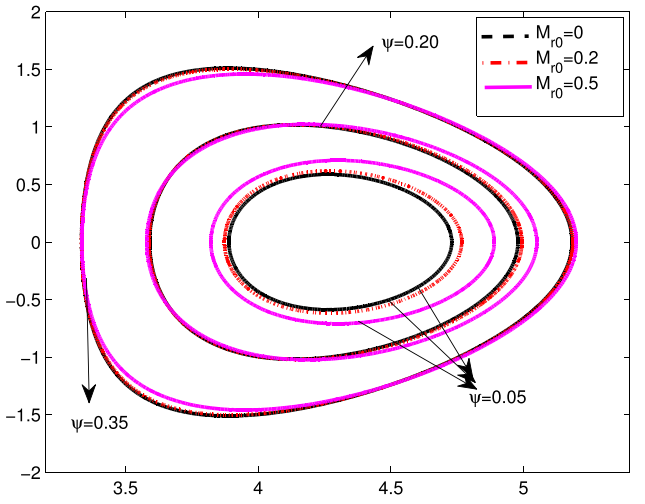

FIG. 3. Increasing shift of the poloidal flux function (and the magnetic axis) with increasing toroidal flow in an EAST-like plasma.

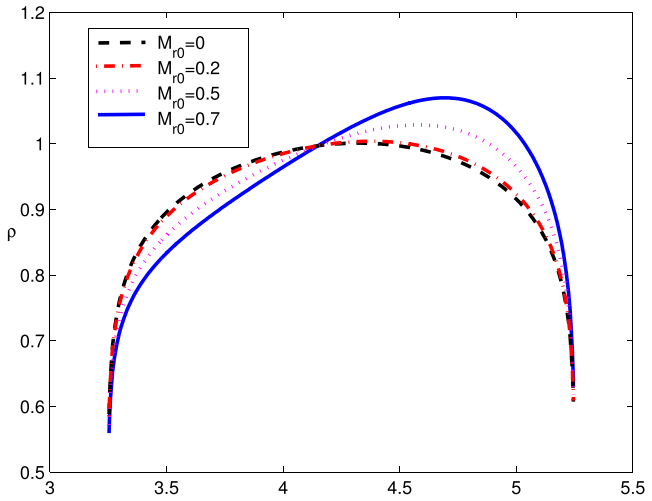

FIG. 4. Normalized density profile across the midplane for varying toroidal flows in an EAST-like plasma.

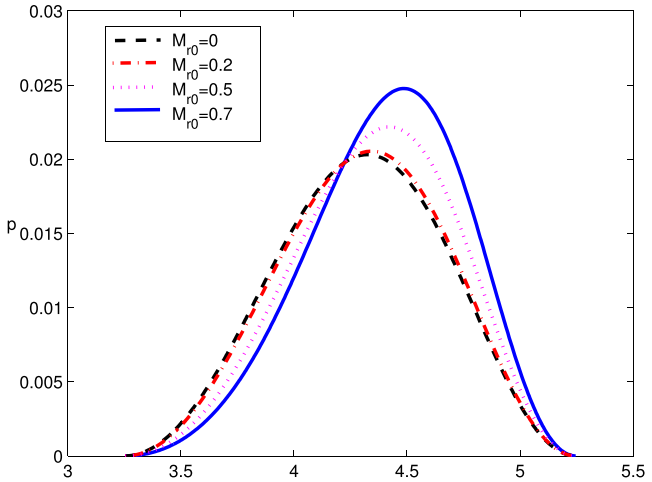

FIG. 5. Profiles of the normalized pressure across the midplane for different amounts of plasma toroidal flow.

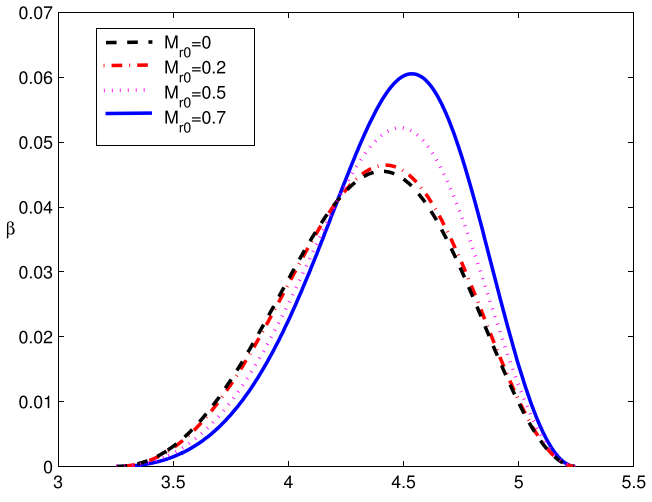

FIG. 6. Profiles of β across the midplane for different amounts of toroidal flow.

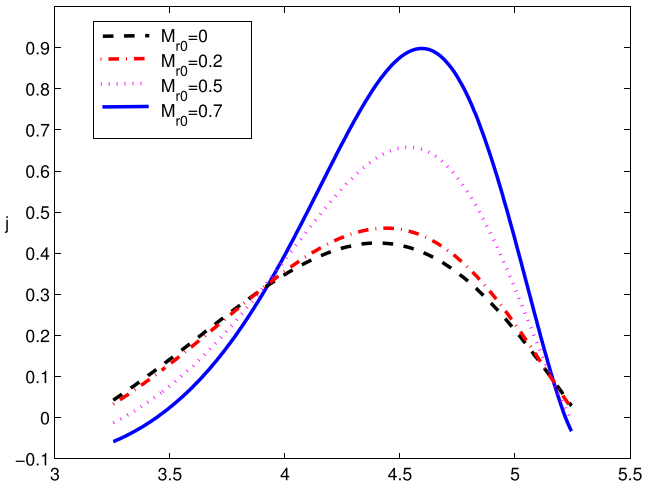

FIG. 7. Profiles of the normalized toroidal current density across the midplane for different amounts of toroidal flow.

$$\beta_N = 100 \times \frac{\beta_v B_0 a \langle B_\varphi \rangle}{I_p} (\%\mathrm{mT/MA}),$$

$$I_p = 10^{-6} \times \frac{B_0 a}{\mu_0} \int j_\varphi dx dz (\mathrm{MA}),$$

where $\langle \cdots \rangle = \frac{\int \cdots dV}{\int dV}$, $dV = 2\pi x dx dz$, and μ_0 is the vacuum magnetic permeability.

The volume averaged global parameters are observed not to have changed much within this series of variation in the rotation Mach numbers. It shows that the plasma equilibrium has compensating changes in the pressure value versus the volume elements across the plasma.

B. Current reversal equilibrium configurations

1. Change in flux function topology (from NEC to CREC) for an equilibrium with low plasma current

For studying the current reversal equilibrium, we first focus our attention on a case when the normalized plasma current is small, with $|I| \ll 1$. Because the total current is very small, fixing the total current becomes a constraint difficult to impose. We first relax this constraint. We fix our attention on the effect of rotation to the change in plasma equilibrium. We take the profiles of the free functions as follows:

$$\frac{dF^2}{d\psi} = b_1 + b_2 \psi, \tag{38}$$

TABLE II. β_v, p_v, β_N, and I_p for NECs with different M_0.

M_{r0}	0	0.2	0.5	0.7
β_v	0.0109	0.0109	0.0107	0.0109
p_v	0.0051	0.0050	0.0048	0.0048
β_N	1.3778	1.3651	1.3398	1.3610
I_p	0.7162	0.7162	0.7162	0.7162

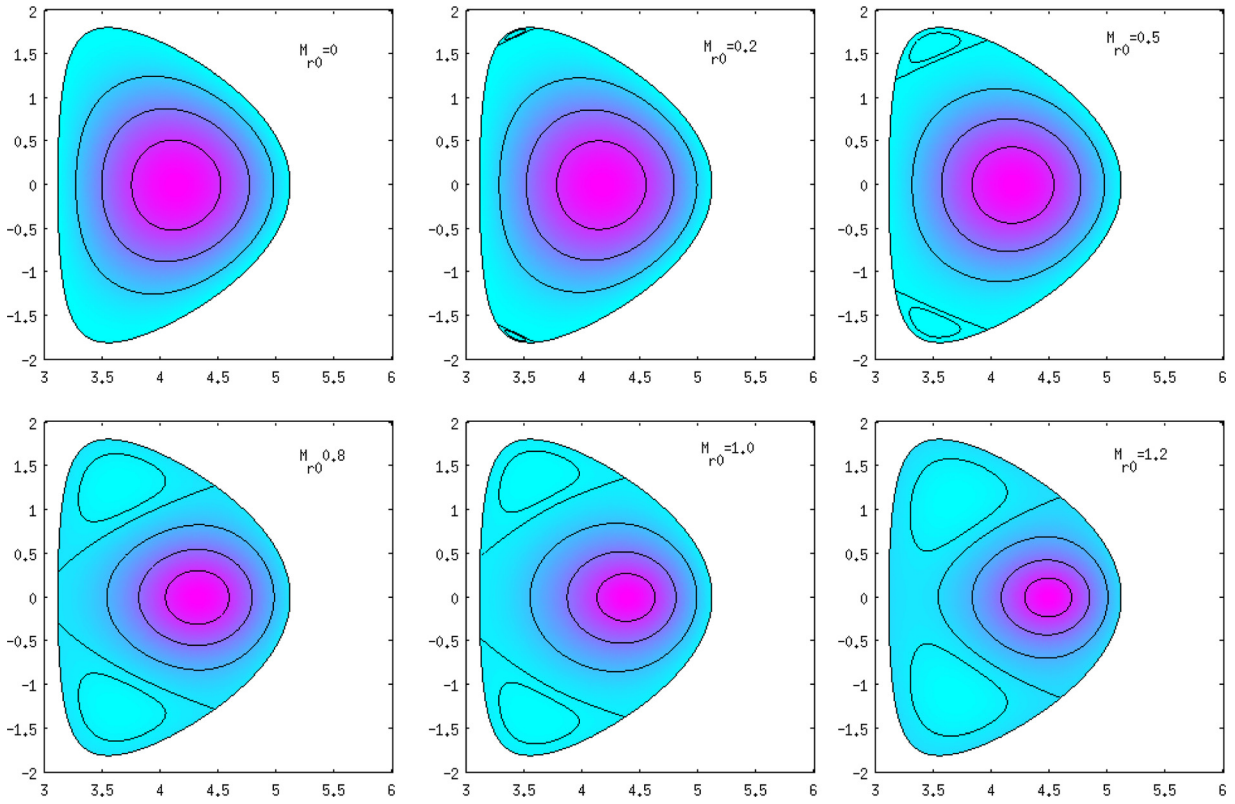

FIG. 8. Magnetic flux surfaces change from NECs to CRECs with increasing Mach number.

$$M = M_e + (M_0 - M_e)\left|\frac{\psi}{\psi_c}\right|^{\mu_M}, \tag{39}$$

$$D = D_e + (D_0 - D_e)\left|\frac{\psi}{\psi_c}\right|^{\mu_D}, \tag{40}$$

$$P = P_e + P_f|\psi|, \tag{41}$$

where ψ_c is the maximum of $|\psi|$. P_f and b_2 are free parameters.

The input parameters for the free functions are taken as $D_e = 0, D_0 = 1, M_e = 0, P_e = 0, b_1 = -0.35, b_2 = 5$, P_f=0.001, $\mu_M = 2$, and $\mu_D = 2$. In this type of profile, both the density and the rotation have gradients extending to the plasma edge. It is found that the plasma equilibrium configuration may change from a NEC into a CREC, which are showed in Fig. 8 by simply varying the value of M_0. In Fig. 8, it is seen that with increasing flow Mach number, the current density on the high field side (HFS) started to become negative. The trend increases with the increase in the flow Mach number. This can be explained by the fact that the effect of toroidal rotation gradients act as an enhanced pressure gradient, with an even higher dependence on the major radius. Large pressure

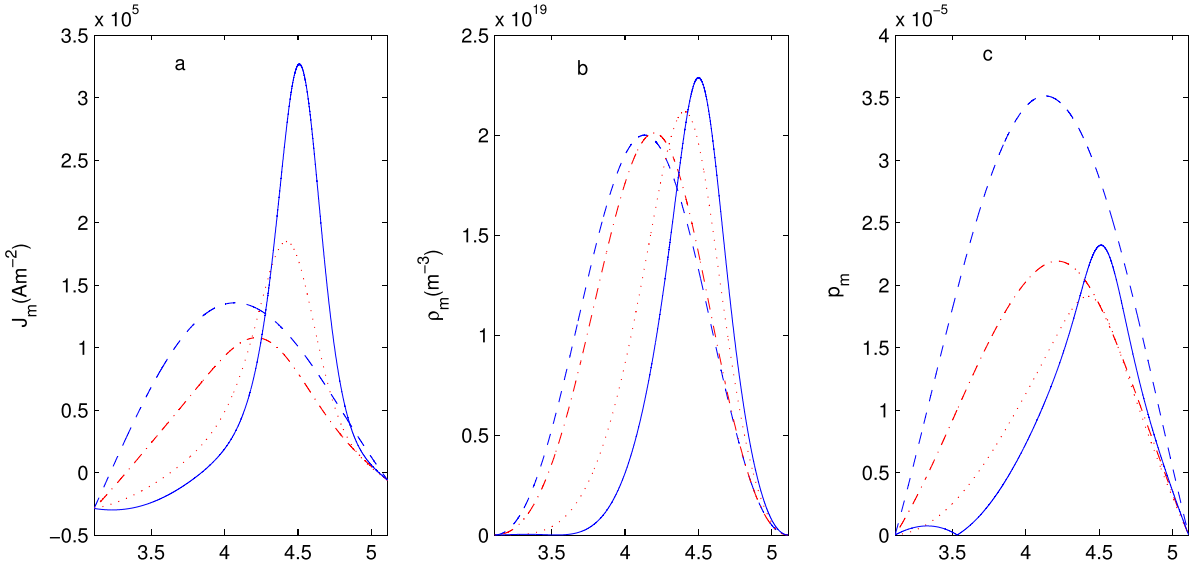

FIG. 9. Profiles of current density J_m, plasma particles density ρ_m, and normalized pressure p_m in the midplane change with varying toroidal flow Mach number when all of parameters of the free functions are fixed except the Mach number (dash: $M_{r0} = 0$, dash dot: $M_{r0} = 0.5$, dot: $M_{r0} = 0.9$, solid: $M_{r0} = 1.2$).

TABLE III. β_v, p_v, β_N of CRECs change with different M_{r0} when keep $I = -0.4 (I_p = -0.2865\,\text{MA})$.

M_{r0}	0	0.5	1.0	2.0
β_v	1.7639×10^{-03}	1.9103×10^{-03}	2.5445×10^{-03}	5.3554×10^{-03}
p_v	9.3697×10^{-04}	1.0070×10^{-03}	1.3415×10^{-03}	4.2576×10^{-03}
β_N	5.8030×10^{-01}	6.2822×10^{-01}	8.4507×10^{-01}	$2.0248 \times 10^{+00}$

gradients near the edge have been known to lead to current reversal near the inside edge of the plasma. Therefore, a large gradient in rotation can more easily lead to a current reversal. Of course, this effect increases with the increase of the rotation Mach number. When the total current is small, the poloidal magnetic field is weak throughout. It is very easy for the plasma to create local closed flux regions (islands). Figs. 9(a) and 9(b) show that the current density and mass density across the midplane change with the change in flow Mach number. It is seen that the trend of these changes is similar to those in the NECs. Fig. 9(c) shows the change in the pressure across the midplane for different flow Mach numbers. It is seen that apart from the outward shift of the pressure profile, a secondary pressure peak appears together with the increase in the flow Mach number.

Table III shows both β_v and p_v decrease monotonically with increasing Mach number. It is seen that all these global parameters are relatively small, except the value of β_N, which is somewhat meaningless because it is normalized with respect to the total current. We would like to comment that the change in topology has not been expected at first. It is, however, easily rationalized as explained above. Furthermore this may correspond to situations in the early low current phase of the tokamak discharge with an intense tangential neutral beam injection. The change in plasma topology can be traced completely to the increase in plasma rotation.

2. Change in flux function topology with fixed total current

Next, we continue with the CREC with a large toroidal current. For this series, we keep the total plasma current constant. We start with a value of P_f and use the chosen imposed normalized total toroidal current I to obtain the value of b_2. It is found that current reversal equilibrium with flow will occur when we assign the input parameters for the free functions as follows: $D_e = 0, D_0 = 1, M_e = 0, P_e = 0, b_1 = -0.05, P_f = 0.005, \mu_M = 0.2$, and $\mu_D = 0.1$. We obtained a series of values of b_2 for different Mach numbers while keeping the normalized plasma current at $I = -0.4$. The results are shown in the following figures.

In Fig. 10, we see that the equilibrium magnetic flux surfaces change from a configuration with three-magnetic-islands into one with two-magnetic-islands when the toroidal Mach number is increased. It is worth noticing that with the increase in the toroidal Mach number, the magnetic island on the inboard side undergoes quite a significant change in shape of its magnetic surfaces, while the magnetic axis undergoes only a minor outward shift. Whereas both of the magnetic islands on the top and bottom gradually merge into one centered on the outboard midplane.

In Figure 11 are shown the change in the normalized toroidal current density across the midplane for the various toroidal flows in the above sequence of CRECs. It is seen that the toroidal current density changed remarkably with the increasing Mach numbers. From Figs. 11(b) and 11(c), it is seen that the plasma density and pressure undergo outward-shifts in each magnetic island in this sequence of CRECs. The peak density and pressure increase with increasing toroidal flow, which is the same as the case for the rotating NECs. Table IV shows p_v, β_v, β_N of this sequence of CRECs all increases with the increase in the Mach number monotonically, which is different from the case of the series of rotating NECs studied in the Subsection III B 1.

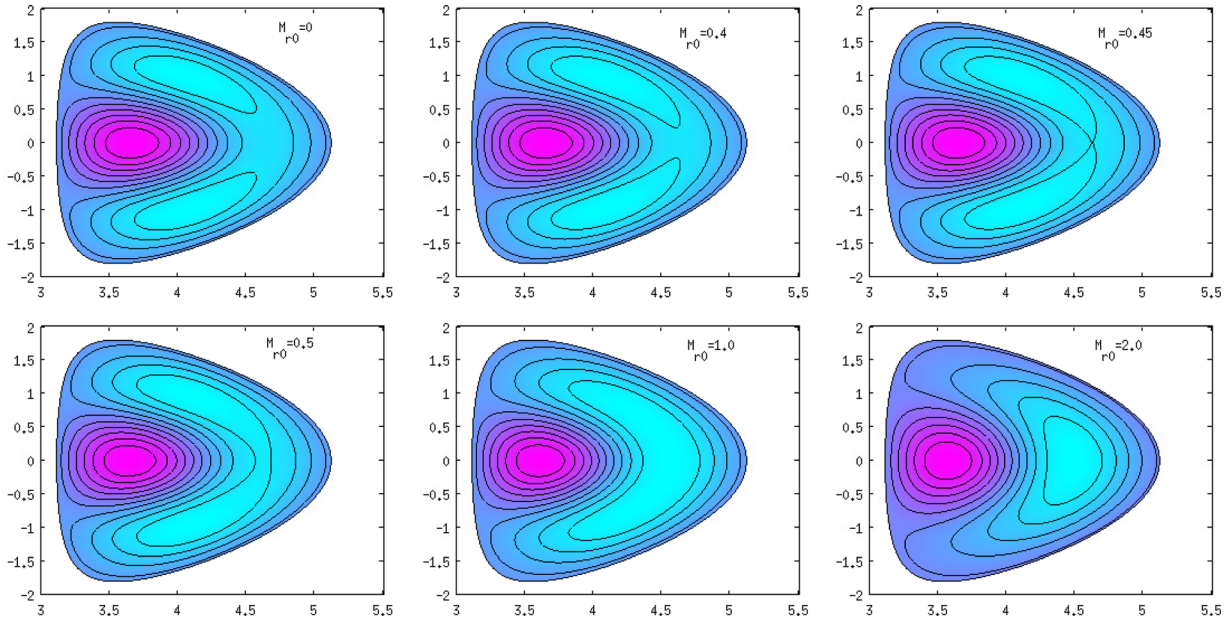

FIG. 10. Magnetic flux surfaces of CRECs change with varying toroidal flow Mach number.

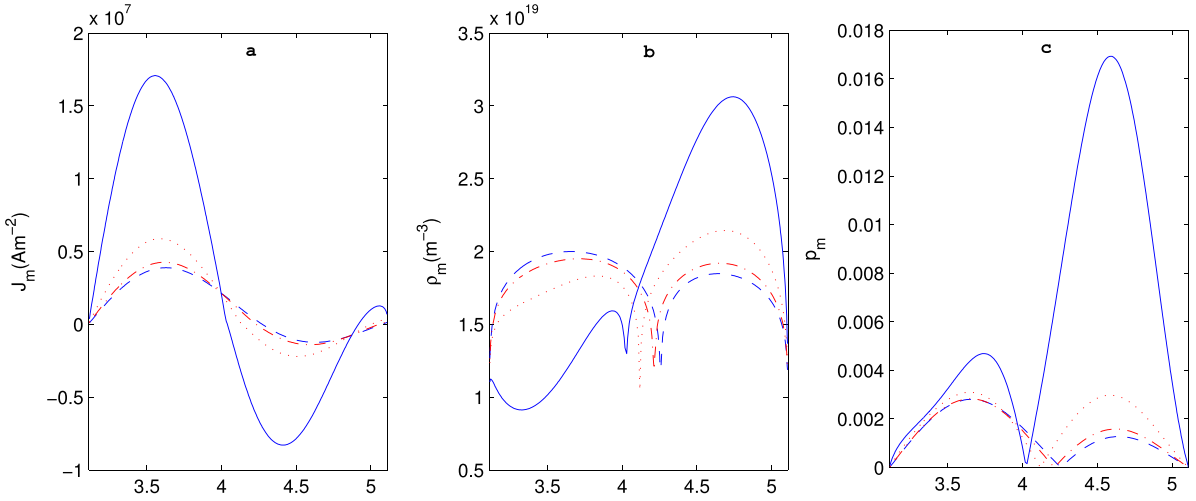

FIG. 11. Profiles across the midplane of CRECs of the current density J_m, plasma particles density ρ_m, and normalized pressure p_m for different toroidal flow Mach numbers when the plasma current is fixed at $I_p = -0.2865$ MA (dash: $M_{r0} = 0$, dash dot: $M_{r0} = 0.5$, dot: $M_{r0} = 1.0$, solid: $M_{r0} = 2.0$).

TABLE IV. Change in β_v, p_v, β_N and I_p for different M_{r0}.

M_0	0	0.5	0.8	0.9	1.0	1.2
β_v	2.6567×10^{-05}	1.4496×10^{-05}	9.3297×10^{-06}	8.3817×10^{-06}	7.8871×10^{-06}	7.5998×10^{-06}
p_v	1.3178×10^{-05}	7.0407×10^{-06}	4.3399×10^{-06}	3.8405×10^{-06}	3.5777×10^{-06}	3.4477×10^{-06}
β_N	5.8225×10^{-02}	8.4194×10^{-02}	2.3502×10^{-01}	1.4285×10^{00}	4.0920×10^{-01}	1.6266×10^{-01}
I_p(MA)	4.2504×10^{-02}	1.6038×10^{-02}	4.1887×10^{-03}	5.4656×10^{-04}	-1.7954×10^{-03}	-4.3521×10^{-03}

IV. SUMMARY AND DISCUSSION

Plasma rotation has been found to affect the stability and transport behavior of the tokamak. However, the study of plasma stability and transport has to start with a self-consistent equilibrium. Therefore, we are motivated to study the effect of toroidal flow on the toroidally symmetric plasma.

We start with the formulation of the equilibrium problem in Sec. II. We derived the Generalized Grad Shafranov equation and discussed our method of solution. The choice of unstructured grid using triangular shaped finite elements allows us to study change in plasma topology with different input profile parameters.

The numerical results are given in Sec. III. First, we validate our results against the known analytic results in the literature. Next, we study the effects of the toroidal flow on a NECs and a CRECs prescribing a EAST-like plasma boundary. For the NEC configuration, the generalized Grad-Shafranov equation is solved with the constraint of fixed total plasma current. It is found that an increase in toroidal flow leads to an increase in the outward shift of the profiles of the density, pressure, β, and toroidal current density across the midplane of the plasma. The shifts become non-negligible when the Mach number is larger than 0.5. These findings all agree with the general findings from previous numerical studies.

Next, the effects of the plasma toroidal flow on the current reversed equilibrium configurations are also investigated. First, we studied a series when the total plasma current is small. It is found that increased plasma rotation can lead to a change of the plasma equilibrium from an NEC to a CREC; in this case, the rotation profile has a finite gradient at the plasma edge. We can directly identify the increase in the rotation value as the cause of the topological change. This could correspond to the experimental situation during the early phase of the plasma discharge when the total current is small, while the plasma undergoes an intense tangential neutral beam injection. Next, we study the change of plasma topology for a CREC plasma with the total discharge current fixed. We found that similar to the low current case, the topology of the flux function can still be modified by changing the toroidal flow. In particular, the plasma topology is shown to change from a configuration with 3 closed magnetic flux regions (islands) to one with just two magnetic islands.

ACKNOWLEDGMENTS

The authors would like to thank Professor M. S. Chu for going through the manuscript and making improvements. They would also like to thank him for his valuable suggestions and comments and Dr. W. F. Guo for useful discussions. One of the authors (Yemin Hu) would like to thank his host Professor Heiji Sanuki for his kindness, hospitality, valuable discussions, help, and arrangements during the whole time of his visit to NIFS. This work was supported by the program of Fusion Reactor Physics and Digital Tokamak with the CAS "One-Three-Five" Strategic Planning, the National Natural Science Foundation of China under Grant No. 11375234 and also partly by National Magnetic Confinement Fusion Science Program of China

under Contract No. 2015GB101003. The authors would also like to acknowledge the ShenMa High Performance Computing Cluster at the Institute of Plasma Physics, Chinese Academy of Sciences.

[1]L. Guazzotto, R. Betti, J. Manickam, and S. Kaye, Phys. Plasmas **11**, 604 (2004).
[2]R. C. Isler, L. E. Murray, E. C. Crume, C. E. Bush, J. L. Dunlap, P. H. Edmonds, S. Kasai, E. A. Lazarus, M. Murakami, G. H. Neilson, V. K. Paré, S. D. Scott, C. E. Thomas, and A. J. Wootton, Nucl. Fusion **23**, 1017 (1983).
[3]R. J. Taylor, J.-L. Gauvreau, M. Gilmore, P.-A. Gourdain, D. J. LaFonteese, and L. W. Schmitz, Nucl. Fusion **42**, 46 (2002).
[4]K. Brau, M. Bitter, R. J. Goldston, D. Manos, K. McGuire, and S. Suckewer, Nucl. Fusion **23**, 1643 (1983).
[5]N. C. Hawkes and N. J. Peacock, Nucl. Fusion **25**, 971 (1985).
[6]M. G. Bell, Nucl. Fusion **19**, 33 (1979).
[7]Y. Shi, G. Xu, F. Wang, M. Wang, J. Fu, Y. Li, W. Zhang, J. Chang, B. Lv, J. Qian, J. Shan, F. Liu, S. Ding, and B. Wan, Phys. Rev. Lett. **106**, 235001 (2011).
[8]S. Suckewer, H. P. Eubank, R. J. Goldston, E. Hinnov, and N. R. Sauthoff, Phys. Rev. Lett. **43**, 207 (1979).
[9]E. K. Maschke and H. Perrin, Plasma Phys. **22**, 579 (1980).
[10]E. Hameiri, Phys. Fluids **26**, 230 (1983).
[11]R. A. Clemente and R. Farengo, Phys. Fluids **27**, 776 (1984).
[12]R. Iacono, A. Bondeson, F. Troyon, and R. Gruber, Phys. Fluids B **2**, 1794 (1990).
[13]A. G. Peeters, Phys. Plasmas **5**, 763 (1998).
[14]F. L. Hinton and M. N. Posenbluth, Plasma Phys. Controlled Fusion **41**, A653–A662 (1999).
[15]F. L. Waelbroeck, Phys. Plasmas **3**, 1047 (1996).
[16]C. Wahlber and A. Bondeson, Phys. Plasmas **7**, 923 (2000).
[17]J. P. Graves, R. J. Hastie, and K. I. Hopcraft, Plasma Phys. Controlled Fusion **42**, 1049 (2000).
[18]A. Sen, D. Chandra, and P. Kaw, Nucl. Fusion **53**, 053006 (2013).
[19]M. W. Kissick, J. N. Leboeuf, S. C. Cowley, and J. M. Dawson, Phys. Plasmas **8**, 174 (2001).
[20]R. Betti and J. P. Freidberg, Phys. Plasmas **5**, 3615 (1998).
[21]D. J. Ward and A. Bondeson, Phys. Plasmas **2**, 1570 (1995).
[22]M. S. Chu, J. M. Greene, T. H. Jensen, R. L. Miller, A. Bondeson, R. W. Johnson, and M. E. Manuel, Phys. Plasmas **2**, 2236 (1995).
[23]K. P. Wessen and M. Persson, Phys. Plasmas **45**, 267 (1991).
[24]H. F. Tammen, A. J. H. Donne, H. Euringer, and T. Oyevaar, Phys. Rev. Lett. **72**, 356 (1994).
[25]V. Varadarajan and G. H. Miley, J. Comput. Phys. **123**, 415 (1996).
[26]H. Tasso and G. N. Throumoulopoulos, Phys. Plasmas **5**, 2378 (1998).
[27]J. A. Breslau, S. C. Jardin, and W. Park, Phys. Plasmas **10**, 1665 (2003).
[28]J. Huang, X. Yang, S. Zheng, C. Feng, H. Zhang, and L. Wang, Nucl. Fusion **40**, 2023 (2000).
[29]M. S. Chu and P. B. Parks, Phys. Plasmas **9**, 5036 (2002).
[30]A. A. Martynov, S. Yu.Medvedev, and L. Villard, Phys. Rev. Lett. **91**, 24 (2003).
[31]S. Wang, Phys. Rev. Lett. **93**, 155007 (2004).
[32]Y. Hu, Phys. Plasmas **15**, 022505 (2008).
[33]S. Yu. Medvedev, Y. Hu, A. A. Martynov, and L. Villard, in *36th EPS Conference on Plasma Physics, June 29–July 3, Sofia 2009 ECA, 2009*, Vol. 33E, P-1.130.
[34]E. Strumberger, S. Günter, J. Hobirk, V. Igochine, D. Merkl, E. Schwarz, and C. Tichmann, ASDEX Upgrade Team, Nucl. Fusion **44**, 464 (2004).